Assessing the Nature of Lipid Raft Membranes

Perttu S. Niemelä[1,2*], Samuli Ollila[1,2], Marja T. Hyvönen[1,2,3], Mikko Karttunen[4], Ilpo Vattulainen[1,5,6,7]

1 Laboratory of Physics, Helsinki University of Technology, Helsinki, Finland, 2 Helsinki Institute of Physics, Helsinki University of Technology, Helsinki, Finland, 3 Wihuri Research Institute, Helsinki, Finland, 4 Department of Applied Mathematics, The University of Western Ontario, London, Ontario, Canada, 5 Memphys Center for Biomembrane Physics, University of Southern Denmark, Odense, Denmark, 6 Physics Department, University of Southern Denmark, Odense, Denmark, 7 Institute of Physics, Tampere University of Technology, Tampere, Finland

The paradigm of biological membranes has recently gone through a major update. Instead of being fluid and homogeneous, recent studies suggest that membranes are characterized by transient domains with varying fluidity. In particular, a number of experimental studies have revealed the existence of highly ordered lateral domains rich in sphingomyelin and cholesterol (CHOL). These domains, called functional lipid rafts, have been suggested to take part in a variety of dynamic cellular processes such as membrane trafficking, signal transduction, and regulation of the activity of membrane proteins. However, despite the proposed importance of these domains, their properties, and even the precise nature of the lipid phases, have remained open issues mainly because the associated short time and length scales have posed a major challenge to experiments. In this work, we employ extensive atom-scale simulations to elucidate the properties of ternary raft mixtures with CHOL, palmitoylsphingomyelin (PSM), and palmitoyloleoyl-phosphatidylcholine. We simulate two bilayers of 1,024 lipids for 100 ns in the liquid-ordered phase and one system of the same size in the liquid-disordered phase. The studies provide evidence that the presence of PSM and CHOL in raft-like membranes leads to strongly packed and rigid bilayers. We also find that the simulated raft bilayers are characterized by nanoscale lateral heterogeneity, though the slow lateral diffusion renders the interpretation of the observed lateral heterogeneity more difficult. The findings reveal aspects of the role of favored (specific) lipid–lipid interactions within rafts and clarify the prominent role of CHOL in altering the properties of the membrane locally in its neighborhood. Also, we show that the presence of PSM and CHOL in rafts leads to intriguing lateral pressure profiles that are distinctly different from corresponding profiles in nonraft-like membranes. The results propose that the functioning of certain classes of membrane proteins is regulated by changes in the lateral pressure profile, which can be altered by a change in lipid content.

Introduction

The understanding of lipid membrane structures and their role in cellular functions has developed significantly since the introduction of the classical fluid-mosaic model by Singer and Nicolson [1]. The fluid-mosaic model predicted that cellular membranes are fluid and characterized by random distribution of molecular components in the membrane, resulting in lateral and rotational freedom. The more recent picture is considerably more elaborate, however. A large number of experimental results converge toward the idea that lateral domains enriched in sphingomyelin (SM) and cholesterol (CHOL) exist in biological membranes. These nanosized domains, called functional lipid rafts, have been suggested to take part in various dynamic cellular processes such as membrane trafficking, signal transduction, and regulation of the activity of membrane proteins [2–4]. The existence of stable lipid rafts in biological membranes is under intense scrutiny, and their existence is actually under debate since the lipid rafts, if they do exist, are probably too small to be resolved by techniques such as fluorescence microscopy [5]. Direct evidence of rafts in vivo is mainly based on monitoring the motions of membrane proteins [6] or on differential partitioning of fluorescent probes in membrane environments [7]. It is, however, difficult to perform experiments using living cells, which complicates measurements of physical quantities of the rafts, such as the exact lipid composition, characteristic size, and lifetime [8,9]. In model membranes, the coexistence of domains in the

liquid ordered (l_o) and the liquid disordered (l_d) phase is widely accepted [9,10]. For example, the l_d phase may be formed by an unsaturated phosphatidylcholine (PC), while the formation of the l_o phase is promoted by a mixture of SM and CHOL. As for rafts, the current understanding of lipid rafts in biological membranes suggests a granular structure of nanometer-scale domains of various compositions [9,11,12] rather than a large-scale phase separation.

The exact nature of the underlying interactions that lead to lipid immiscibilities in membranes is under debate [13,14]. CHOL is particularly important as it has been shown to increase the conformational order of acyl chains and reduce the bilayer area, hence significantly increasing the packing density of the lipids [15–17]. CHOL is particularly effective in

Abbreviations: A, average area per lipid; CHOL, cholesterol; d, bilayer thickness; D, lateral diffusion coefficient; K_A, area compressibility modulus; k_BT, thermal energy scale (k_B is the Boltzmann constant, T is the absolute temperature); k_c, bending rigidity; l_d, liquid disordered phase; l_o, liquid ordered phase; PC, phosphatidylcholine; POPC, palmitoyloleoylphosphatidylcholine; PSM, palmitoylsphingomyelin; S_{CD}, deuterium order parameter values; SM, sphingomyelin

* To whom correspondence should be addressed. E-mail: psn@fyslab.hut.fi

Author Summary

Biological membranes are complex 2-D assemblies of various lipid species and membrane proteins. For long, it was thought that the main role of lipid membranes is to provide a homogeneous, liquid-like platform for membrane proteins to carry out their functions as they diffuse freely in the membrane plane. Recently, that view has changed. It has become evident that several lipid environments with different physical properties may coexist, and that the properties of the different lipid domains may play an active role in regulating the conformational state and dynamic sorting of membrane proteins. We have carried out atom-scale computer simulations for three-component lipid bilayers, so-called lipid rafts, rich in cholesterol and sphingolipids. They show that arising from the local interactions between the lipid species, the elastic and dynamic properties of the membranes depend strongly on the lipid composition. The changes in elastic properties are suggested to alter the functional states of various membrane proteins. Changes in lipid composition are also shown to alter the distribution of local pressure inside the membrane. This is likely to affect proteins that undergo large anisotropic conformational changes between the functional states, such as the ion channel MscL, used as an example here. A great number of important physiological phenomena, such as transmitting neural impulses or trafficking molecules in and out of the cell, involve activation of membrane proteins, so it is relevant to understand all factors affecting them. Our findings support the idea that general physical properties of the lipid environment are capable of regulating membrane proteins.

reducing the void space within the acyl chain region of the lipids [15], which is related to suppressed area compressibility and increased bending rigidity of the membrane with increasing CHOL concentrations. However, the lateral diffusion rates are not expected to slow down by more than a factor of 2–3 when the l_d phase is compared with CHOL-induced l_o phase [6,18]. Also, CHOL has recently been reported to significantly alter the lateral pressure profile of membranes [19]. This is important, as changes in the lateral pressure profiles have been suggested to be related to changes in membrane protein structure and activity [20].

Considering that the smallest estimates for the sizes of rafts fall in the range of nanometers [21,22], they make an accessible subject for computational studies. Though, in spite of the considerable importance of rafts, it is somewhat surprising that only a few atom-scale simulations have dealt with ternary mixtures of CHOL, SM, and PC [23,24], concentrating mainly on small-scale structural properties and local interactions between the lipids. In particular, there are no previous atom-level computational studies of rafts aiming to characterize the nature of their structural and dynamical features. For example, the nanometer scale structure within raft domains and its interplay with CHOL-induced effects are not understood. Further, the resulting large-scale properties, such as membrane elasticity in ternary raft-like lipid mixtures, are not understood either. Finally, and perhaps most importantly, the lateral pressure profiles associated with rafts are completely unknown. The concept of the lateral pressure profile across the lipid membrane is exceptionally significant, since it describes the pressure exerted on molecules embedded in a membrane. Cantor has proposed that incorporation of molecules into membrane and changes in lipid content would alter the lateral pressure

profile across a membrane, and hence changes in the pressure profile would induce changes in membrane protein structure [20,25]. Experimental studies of this issue are remarkably difficult, however: currently there is only one study that employed fluorescent probes to gauge the overall shape of the lateral pressure profile [26]. Evidently, detailed atomistic simulations are called for.

The state-of-the-art extent of the simulations conducted in this work, 15–20 nm in lateral dimensions and 100 ns in time, enables a reliable quantitative analysis of the properties of raft-like membranes not accomplished before. We employ large-scale atom level simulations for three mixtures of palmitoyloleoylphosphatidylcholine (POPC), PSM, and CHOL. The molar fractions are POPC:PSM:CHOL = 1:1:1, 2:1:1, and 62:1:1 for systems that we call S_A, S_B, and S_C, respectively (see Figure 1). Based on a recent experimental phase diagram [27], these mixtures are expected to display the coexistent l_o and l_d phase domains (S_A and S_B) or a single l_d phase (S_C). Here, we illustrate the distinct nature of raft-like domains in three parts. First, we consider the elastic, thermodynamic, and dynamic properties of rafts that turn out to be very different from those of nonraft-like membranes. Second, we provide evidence that the presence of PSM and CHOL in raft-like membranes leads to strongly packed and rigid bilayers, characterized by significant nano-scale lateral heterogeneity within the raft domains. These findings express the prominent role of favored lipid–lipid interactions within rafts and highlight the significant role of CHOL in promoting the formation of rafts. Third, we provide compelling evidence that the lateral pressure profiles can be altered by a change in lipid content. In particular, we show how the presence of PSM and CHOL leads to intriguing lateral pressure profiles that are distinctly different from corresponding lateral pressure profiles in nonraft-like membranes, proposing that lipid membranes may regulate the functioning of certain classes of membrane proteins such as mechanosensitive channels through changes in lipid composition, and hence the lateral pressure profile.

Results

Elastic, Thermodynamic, and Dynamic Properties

Selected properties of the simulated membranes are summarized in Table 1. For system S_C, the average area per lipid, A, and the bilayer thickness, d, are in agreement with previous findings on pure POPC bilayers [28,29], indicating negligible effects of PSM and CHOL on the bilayer dimensions. Also, the area compressibility modulus, K_A, and the bending rigidity, k_c, are in line with previous studies of pure PC bilayers, reporting $K_A = 140–300 \times 10^{-3}$ N/m and $k_c = 4–9 \times 10^{-20}$ J [30–32]. The lateral diffusion coefficient, D, for POPC in system S_C is about 50% lower than the value of 1.4×10^{-7} cm^2/s measured for pure POPC bilayer at 313 K [33]. A similar trend was found in comparison of our previous simulations on pure SM and PC bilayers [34] with this particular study [33]. This suggests that bilayer S_C is close to the liquid disordered state of a POPC bilayer. This is also supported by the finding that small CHOL [33] or SM [35] concentrations have minor effects on D values of PC above melting temperatures.

The condensing effect of CHOL becomes evident when comparing the values of A and d between systems S_A to S_C. As
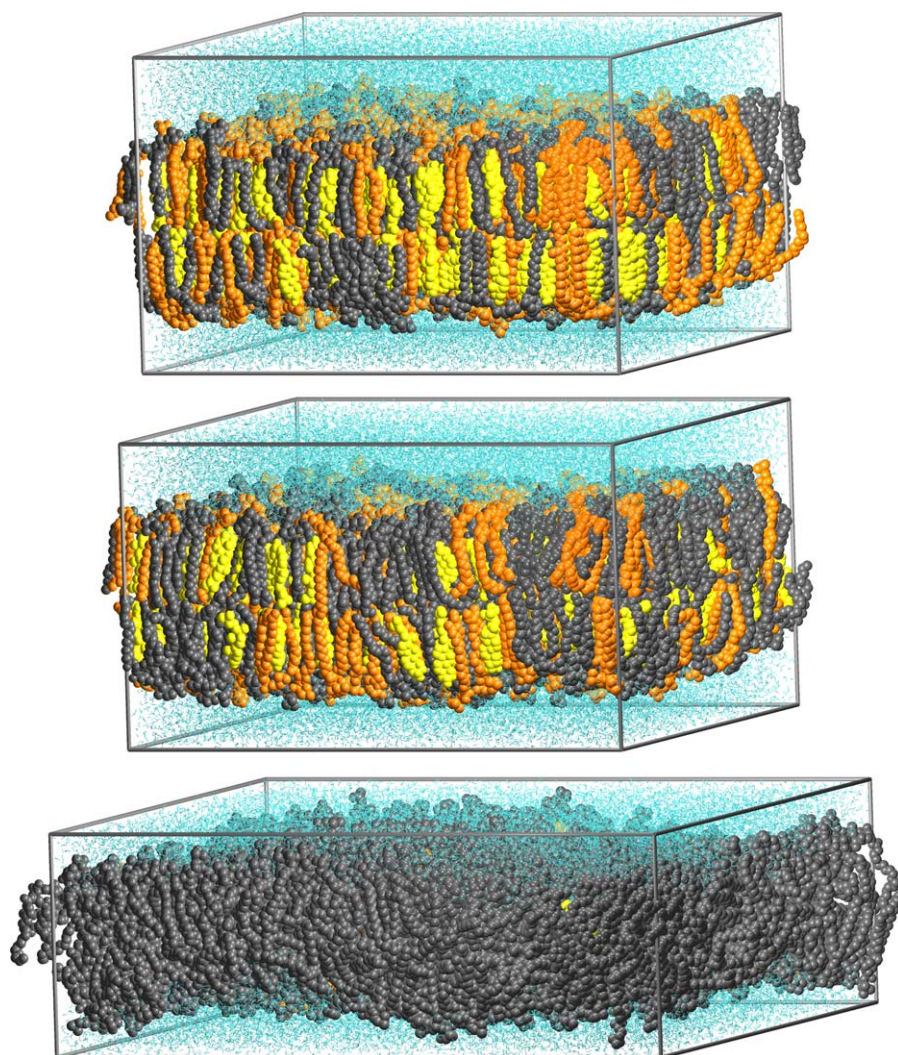
Figure 1. Snapshots at the End of Simulations for Systems S_A (Top), S_B (Middle), and S_C (Bottom)
POPC molecules are shown in gray, PSM in orange, CHOL in yellow, and water in cyan.
doi:10.1371/journal.pcbi.0030034.g001

suggested in several previous works, CHOL's tendency to increase the order of neighboring acyl chains leads to decreased area per lipid and increased bilayer thickness upon increasing CHOL concentration [36–38]. Comparison with previous studies shows that the values for A in Table 1 for S_A and S_B are 0.1–0.4 nm^2 lower than expected for binary PC–CHOL systems with similar CHOL concentrations [15,16]. CHOL's strong tendency to reduce fluctuations and increase the rigidity of membranes is best revealed by the K_A values in Table 1. Previous reports have predicted maximally 5-fold to 7-fold increases in the K_A values upon CHOL addition into PC bilayers [16,39]. The presently found unexpectedly large K_A and small A as compared with PC–CHOL systems suggests an additional effect of PSM to decrease area fluctuations, possibly related to the tendency of SM to form intermolecular hydrogen bonds [34,40]. This idea is further supported by an experiment reporting a much higher value of K_A ($1{,}718 \times 10^{-3}$ N/m) for a SM–CHOL bilayer than the value for a PC–CHOL bilayer ($K_A = 781 \times 10^{-3}$ N/m), both with 50 mol% CHOL [41]. Our values for the bending rigidity, k_c, are roughly in line with experimental results for PC–CHOL mixtures, which have

shown a 120%–170% increase in the k_c value upon increasing CHOL fraction from 0 to 30–50 mol% [31,42]. As the experimental values vary and computational reports on CHOL's effect on k_c values in PC membranes are lacking, a more quantitative evaluation on PSM's effect in this case is difficult. However, its tendency to increase K_A would suggest a role also on bending rigidity.

The fact that our values for the bilayer thickness agree with an AFM study, reporting a difference of 0.6–0.9 nm between l_d and l_o phases, is an indication that our model systems are in line with the experimental l_o/l_d phases [43]. However, when comparing the diffusion coefficients between systems S_A to S_C, we find that systems S_A and S_B are relatively much more slowed down than predicted from the changes of pure POPC bilayer upon addition of 25–30 mol% CHOL [33]. This further supports the idea that SM (together with CHOL) has an additional role in rigidifying the bilayer and consequently slowing down diffusion. For comparison, a recent pulsed-field gradient NMR study [44] reported two populations of D values in DOPC–SM–CHOL mixtures with 10–30 mol% CHOL at 300 K, one corresponding to l_d phase ($D \approx 1 \times$

Table 1. Average Structural and Thermodynamic Properties Calculated from the Simulations of Systems S_A, S_B, and S_C

System	S_A	S_B	S_C
POPC:PSM:CHOL	1:1:1	2:1:1	62:1:1
A [nm²]	0.41 ± 0.01	0.44 ± 0.01	0.66 ± 0.01
d [nm]	4.40 ± 0.05	4.29 ± 0.05	3.53 ± 0.05
K_A [10^{-3} N/m]	2,700 ± 700	1,000 ± 400	200 ± 100
k_c [10^{-20} J]	10 ± 2	7 ± 2	6 ± 2
D_{popc} [10^{-7} cm²/s]	0.037 ± 0.002	0.08 ± 0.02	0.67 ± 0.06
D_{psm} [10^{-7} cm²/s]	0.036 ± 0.002	0.07 ± 0.02	0.8 ± 0.2
D_{chol} [10^{-7} cm²/s]	0.038 ± 0.002	0.08 ± 0.02	0.5 ± 0.2

A, average area per lipid; d, bilayer thickness; K_A, area compressibility modulus; k_c, bending rigidity modulus; D, lateral diffusion coefficients.
doi:10.1371/journal.pcbi.0030034.t001

10^{-7} cm²/s) and the other to l_o phase ($D \approx 1 \times 10^{-8}$ cm²/s). As the exact lipid composition within the proposed domains is unknown, our simulated D values for systems S_A and S_B are in good agreement with the proposed l_o phase. This is interesting, since the l_o phase is usually characterized as having similar diffusion rates with the l_d phase. Recent evidence on large variations in the properties of a single l_o phase [45] also supports the idea that bilayers S_A and S_B do display the l_o phase. Clearly, diffusion within raft domains is strongly suppressed due to the presence of PSM and CHOL.

The material properties of lipid bilayers have been suggested to play a major role in regulating the activity and partitioning of membrane proteins. First, the thickness difference of raft and nonraft membranes may be relevant due to the effects of hydrophobic matching [46,47]. For example, the free energy of opening of a bacterial stretch-activated channel has been observed to change from 4 to 20 k_BT when the acyl chain length of the surrounding PC-lipids changes from 16 to 20 carbons [48]. Another example is the transmembrane protein OmpA, whose free energy of unfolding was reported to change by about 5 k_BT per nm when the hydrophobic thickness of the surrounding saturated PC-membrane was varied [49]. Using this value as a simplistic estimate for the effect of hydrophobic thickness, one gets a difference of about 4 k_BT in the free energy of unfolding when this particular protein would be transferred from nonraft to raft membrane. As the higher bending rigidity of the raft membrane probably decreases the ability of the membrane to adapt its thickness to match the hydrophobic thickness of the protein, the actual value should be larger than the above estimate. The role of membrane elasticity in protein functionality is further emphasized by the fact that, based on recent studies, it costs much more energy to deform a membrane by changing its area per lipid than by bending or chain tilting [50]. It has been suggested that the free energy to create a protein-shaped cavity in a bilayer is proportional to K_A [51], and evidence exists that the binding free energy of certain amphipathic peptides indeed depends linearly on K_A [52]. Our data suggests a 5-fold to 14-fold difference in the values of K_A between raft and nonraft membranes (see Table 1), which practically means a free energy cost of about 4–8 k_BT when a membrane protein (Mellitin) is transferred from a nonraft to a raft environment [52]. Summarizing, the elasticity of raft-like membranes is substantially different

from that of nonraft membranes, and this likely influences membrane protein functionality.

Lateral Heterogeneity

The above results highlight the different bulk properties of raft-like domains with respect to more disordered bilayers. However, as becomes evident below, raft domains are also characterized by strong spatial and temporal variations. Figure 2 reveals lateral heterogeneity in the calculated deuterium-order parameter values (S_{CD}) when averaged over 10 ns. The nature of chain ordering varies in different systems. System S_A exhibits the highest overall order (average $S_{CD} = -0.41$) that is almost uniformly distributed over the bilayer plane and broken only by a few small low-order areas and empty points due to poor sampling. System S_B is slightly less ordered ($S_{CD} = -0.36$) and contains domains of a few nanometers in size, differing significantly in their S_{CD} values. The overall ordering in S_C is much weaker ($S_{CD} = -0.18$) than in the two other systems, but even S_C displays lateral heterogeneity, though the domains appear larger, smoother, and with smaller variations in the S_{CD} values. The average S_{CD} values are in line with corresponding experimental order parameter profiles of fluid POPC [53,54] and DPPC–CHOL mixtures with similar CHOL concentrations [45,55].

In Figure 2, the more ordered regions in S_{CD} plots are clearly correlated with a higher density of CHOL. This is in line with a previous study showing CHOL's ability to order the neighboring acyl chains within a radius of few nanometers [56]. The σ_{chain} plots in Figure 2 reveal high localization of the chains in S_A, whereas in S_B some of the regions are smeared out. The S_C plot is much more homogeneous, indicating higher overall mobility and more isotropic distribution of the chains. In S_C, the small concentration of CHOL does not seem sufficient to account for the observed large-scale lateral heterogeneity in chain-order parameters. Instead, we find that the S_{CD} value is clearly correlated with bilayer thickness. This is particularly supported by the fact that the amplitudes of the large-scale peristaltic wave modes are significantly larger for system S_C than for the other systems (see Figure S6). Even though the autocorrelation functions for most of the largest undulations and peristaltic modes decay roughly within a few nanoseconds (unpublished data), some modes display much longer decay times. In particular for system S_C, this may be related to the heterogeneity induced by the few CHOL and SM molecules that are embedded in the bilayer.

To judge our findings for lateral heterogeneity, it is worthwhile to stress the slow dynamics in the bilayer plane: despite the extensive time scale simulated, the lateral diffusion coefficients indicate that the molecules move in the plane of the membrane approximately over only their own size within the simulated time scale. Hence, it is evident that the simulation time is not long enough to adequately relax the large-scale structure of the initial configuration and lead to complete mixing of the lipids. The nanoscale heterogeneity observed in this work could thus be debated. However, there is reason to emphasize that while systems S_A and S_B were started from different initial configurations, they lead to similar conclusions. Further, the small-scale movements of the molecules relative to each other can be characterized; see the 2-D radial distribution functions in Figure 3. The unfavorable close contacts of CHOL–CHOL
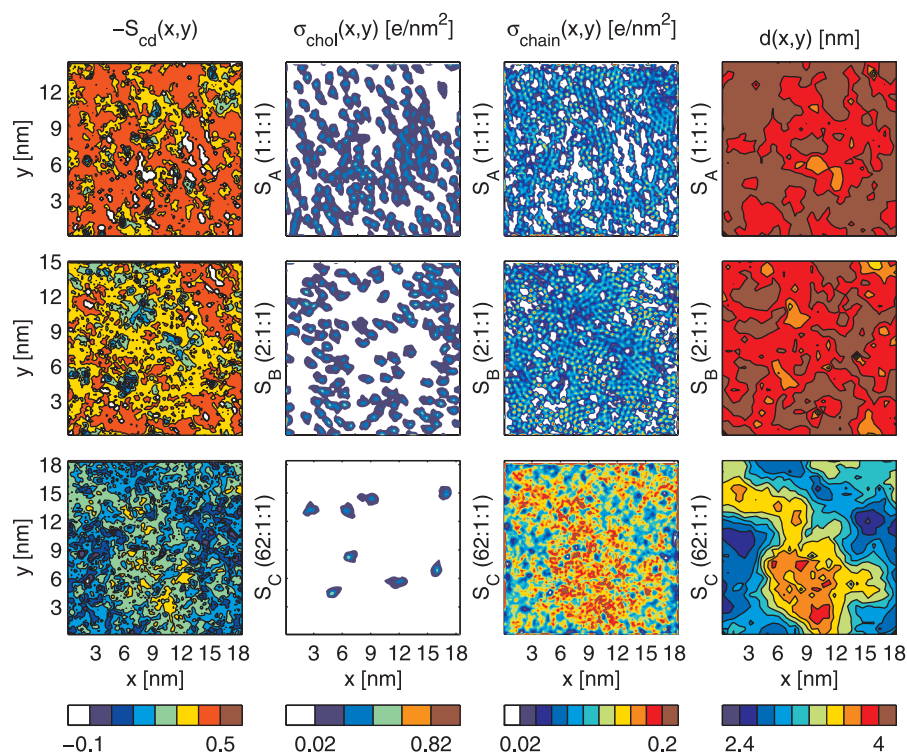
Figure 2. Snapshots Averaged over the Last 10 ns from the End of Each Simulation

The deuterium order parameters, S_{CD}, of selected carbons (C5–C7) of POPC and PSM chains were binned in the xy-plane (column 1, from left). The in-plane electron densities, σ, have been plotted separately for CHOL (column 2) and the selected chain carbons (column 3). The average bilayer thickness, d, was obtained from the grid of the undulation analysis (column 4). Systems S_A to S_C are represented on rows from top to bottom, respectively. Only the bottom leaflet has been used for columns 1–3, whereas both leaflets were used for column 4. The equivalent plots for the top leaflet have been presented in Figure S2.

doi:10.1371/journal.pcbi.0030034.g002

pairs are revealed by the lowering of the nearest neighbor peak in time. Simultaneously, the secondary peak at 1.0 nm increases, indicating small-scale reorganization of CHOL molecules. Significant changes in time can also be seen in the other plots of Figure 3, revealing the tendency of closer contacts between CHOL–POPC center of mass pairs with respect to PSM–CHOL pairs. In all, this provides further support for lateral reorganization and heterogeneity. The details of the lipid–lipid interactions are related to the widely speculated specific interaction between SM and CHOL, which is discussed elsewhere [57,58].

Lateral Pressure Profiles

Structure and dynamics of membrane proteins are likely to be influenced by the lateral pressure profile, which has been proposed as a mechanism for, e.g., general anesthesia [20,59]. To elucidate this issue, we computed the lateral pressure profiles of various lipid membrane systems (see Figure 4). For a discussion of the coupling of the peaks in the lateral pressure profile with the molecular groups and different interaction types, see previous related simulation studies [19,60–63]. Here, we focus on a more generic issue, that is, the joint effect of CHOL and PSM on the pressure profile.

The pressure profiles across the membranes of S_A and S_B, shown in Figure 4A, indicate a striking difference compared with profiles in nonraft membranes (see Figure 4B): raft bilayers display qualitatively different behavior with a greater number of peaks as compared with single component POPC and PSM bilayers in l_d phase. Rather, raft systems display a

qualitative similarity to the DPPC–CHOL system, shown in Figure 4B. These observations are in line with previous simulation studies, if reports on other single component l_d bilayers [60–62] are compared with binary PC–CHOL systems [19,63]. A remarkable difference found here is the significant increase of positive (repulsive) pressure at the middle of raft bilayers compared with pure POPC, the effect being particularly large in the case of raft-mixture S_A.

Notably, the peak heights in the lateral pressure profile are of the order of 1,000 bar. Thus, molecules such as integral membrane proteins are under the influence of huge local pressures that likely affect their conformational state. Particularly, proteins whose cross-sectional area undergoes significant anisotropic changes when shifting from active to inactive state are likely to be governed or regulated by the pressure profile [20,64]. To further quantify this idea, we estimated the lateral pressure profile–induced component of the energy between open and closed conformations of a channel protein MscL (see Methods). For this quantity, we get $\Delta W = (11 \pm 2)\, k_B T$ and $(4 \pm 1)\, k_B T$ for systems S_A and S_B, respectively. These are significantly higher than the values found for the pure POPC bilayer $(1.9 \pm 0.2)\, k_B T$, the pure PSM bilayer $(1.0 \pm 0.6)\, k_B T$, or the binary DPPC–CHOL bilayer $(1.0 \pm 0.4)\, k_B T$. The above result for a POPC bilayer is in agreement with the previous calculation by Gullingsrud and Schulten [62], who found $1.7\, k_B T$ for POPC. The positive values of ΔW indicate that the lateral pressure profiles of these bilayers lower the open state energy of MscL relative to the closed state; that is, they are in favor of the open state.
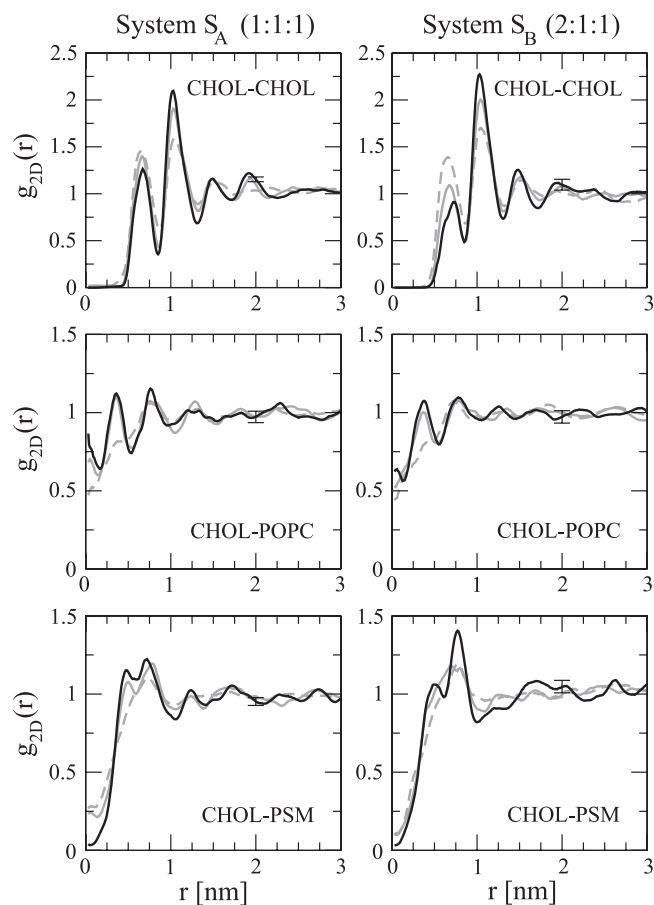
Figure 3. 2-D Radial Distribution Functions between the Molecular Center of Mass Positions in S_A and S_B

The figures show the time evolution in the system at three different time intervals: 0–10 ns (gray, dashed), 30–40 ns (gray), and 90–100 ns (black). The error bars for the black curve indicate the average difference of the two monolayers.

doi:10.1371/journal.pcbi.0030034.g003

Figure 4. Lateral Pressure Profiles of Systems S_A and S_B (Top) and of Previously Simulated Pure POPC/PSM Systems and a Binary DPPC–CHOL System (Bottom)

The center of the membrane is at $z = 0$. The graphs have been averaged to be symmetric on both sides of the center and smoothed by adaptive high-order spline fitting [90]. Error bars are statistical errors for each slab. The errors have been shown for only one of the monolayers of the DPPC–CHOL system because they are equal for both monolayers and also smaller or equal for the other systems.

doi:10.1371/journal.pcbi.0030034.g004

Especially interesting are the large values found for the raft systems, which suggest that the lateral pressure profiles characteristic of raft-like environments would facilitate the opening of MscL. For comparison, it has been estimated that the free energy difference associated with the opening of MscL is about 20–50 $k_B T$ [62,65]. The contribution due to the pressure profile in a raft domain could therefore be significant. In general terms, it is clear from the above estimates that the equilibrium probability of MscL to be in the open state must be significantly altered by the pressure profile of the lipid environment. Additionally, we wish to underline that the values for ΔW have been estimated for different bilayers that are all under identical surface tension conditions ($\gamma = 0$) and are thus not related to the usual picture of the effect of overall stress on mechanosensitive channels.

Discussion

In this work, we have elucidated properties of lipid raft mixtures through atom-scale simulations and compared them with properties of a bilayer in liquid disordered phase. We found that the presence of PSM and CHOL in S_A and S_B not only significantly enhanced the lateral packing of lipids and increased the acyl chain order, but also reduced the lateral
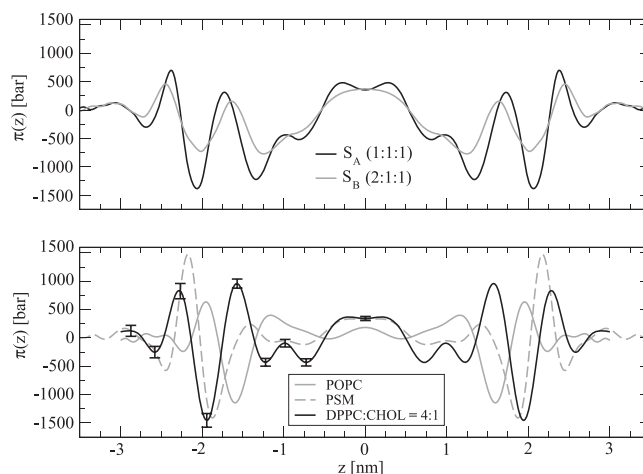
diffusion rates by more than an order of magnitude when compared with the l_d phase. This observation is contradictory to the traditional definition of the l_o phase, but is in agreement with recent reports on varying properties of this particular phase [45,54]. It is interesting to note that the difference in the lipid dynamics of the different phases may in itself have a contribution to the dynamical partitioning of membrane proteins [5], as they spend more time in the ordered domains due to slower diffusion and allow more time for cross-linking between proteins to occur.

The elasticity of the raft mixtures was found to be reduced significantly when compared with S_C. The fact that this reduction was greater than expected from previous reports on binary PC–CHOL mixtures, suggests that SM has a further rigidifying effect on raft mixtures. The 5-fold to 14-fold increase in K_A suggests significant implications on the partitioning of membrane proteins. First, the free energy of creating a cavity to the membrane, and thus the solvation free energy of a protein into a membrane, is directly proportional to K_A, which leads to unfavored partitioning of certain proteins into raft-like membranes. On the basis of a recent experimental report [52], we estimated that the transfer free energy of Mellitin from nonraft to raft membrane would be about 4–8 $k_B T$. Second, the difference in thickness of about 0.8–0.9 nm between raft and nonraft membranes suggests a contribution to the transfer free energy of proteins due to changed hydrophobic matching. This effect is practically always present and the reported strength of the effect, about 5 $k_B T$ per nm [49], makes it comparable to the effect of the K_A.

The lateral heterogeneity in the simulated membranes was found to be related to either the tendency of CHOL to order neighboring acyl chains or to the relatively slow peristaltic modes of the bilayer. The emergence of these heterogeneities may be related to the idea of small granular arrangement of nanodomains in biological membranes [9,12]. Considering the perhaps surprisingly slow diffusion rates observed for the

l_o phase of the ternary mixtures in this study, it suggests an absolute minimum of about 10–100 ns for the lifetimes of the domains. Also, the analysis of the heterogeneity provided more support for the idea that CHOL changes the lipid environment in its local neighborhood, e.g., by increasing the order of the acyl chains.

Analysis of the raft-like membranes S_A and S_B revealed large differences in lateral pressure profiles when compared with bilayers in l_d phase, but also changes of significant magnitude in the local pressure were found in comparison with PC–CHOL systems. All membrane proteins, which undergo anisotropic structural changes between functional states, are likely to be affected by the lateral pressure profile. A good example would be proteins that tilt their helices when opening a channel, such as the MscL [66]. We found that the free energy difference between the open and closed states of the MscL channel changed from 1.0 $k_B T$ to 4–11 $k_B T$ when single component bilayers in l_d phase were compared with raft mixtures. This result, together with previous reports on pressure profiles of similar systems [19,63], provides strong evidence for the idea that the lipid environment plays an important role in regulating the activity of certain membrane proteins through changes in lateral pressure profile. Though only a few experimental studies have been done to assess local pressures within the bilayer [26,67], evidence exists that the activity of a number of membrane proteins is dependent on the lipid composition and thus very probably on the lateral pressure profile [67,68]. For example, the free energy of binding of alamethicin has been reported to be a simple function of monolayer spontaneous curvature [69], which is most probably related to changes in local pressures.

The role of the lipid environment has been discussed in relation to a variety of membrane proteins, from mechano-sensitive channels such as MscL [48,62,70] to other important channels such as rhodopsin [71], KcsA [67], P-glycoprotein [72,73], the insulin receptor [17], and others whose activity has been shown to depend on the membrane composition [67]. It has been shown that different lipids have different binding affinities on the surface of membrane proteins [74] and that the specific lipid-protein interactions probably play a role in regulating the activity and/or partitioning of certain proteins such as the yeast cytochrome bc_1 complex [75]. However, various evidence exists that generic interaction mechanisms in terms of for example elastic properties of the membrane are also important for a number of membrane proteins [47]. For example, different sterols have been shown to alter the elastic properties of membranes in a similar manner, if only applied in different concentrations [76]. Finally, it is exciting to note that the present results also provide support for a recent suggestion that the (unknown) mechanism of general anesthesia is related to changes in the lateral pressure profile due to incorporation of anesthetics, such as alcohols, into the membrane [20,64,77].

From now on, the quest is to understand the (concerted) effect of different lipid species on the lateral pressure profiles and the interplay between lipid environment and protein activity. The lateral pressure profile is an important quantity, as many membrane elastic coefficients (such as bending modulus, spontaneous curvature, and the saddle splay modulus) can be directly extracted from it [78]. In the future, it would be highly useful to see computational works on lipid bilayers that gather enough statistics to evaluate the relation-ship between these quantities and to increase our under-standing of their relationship. Also, it would be highly interesting to develop experimental techniques to measure the pressure profiles and to relate these to the already existing simulation data of different membrane compositions.

Materials and Methods

Starting coordinates were obtained by expanding a previously equilibrated POPC bilayer [28] to 1,024 lipids. Two ternary mixtures were created by replacing random POPC molecules by PSM and CHOL to result in POPC:PSM:CHOL = 1:1:1 or 2:1:1 molar ratios (systems S_A and S_B, respectively), whereas for the third system (S_C) we replaced 32 selected POPC molecules to result in a POPC matrix with eight CHOL-PSM dimers and 16 monomers that are as far as possible from each other. The configuration in S_C was created to study the local interactions between PSM and CHOL in a POPC matrix, which will be discussed elsewhere [58]. The force-field parameters for POPC [79], PSM [34], and CHOL [80] were obtained from previous works. Each of the three bilayers were fully hydrated with about 28 SPC (simple point charge) water molecules/lipid [81], resulting in ~140,000 atoms per system (see Figure 1). Using GROMACS (http://www.gromacs.org) [82] for integrating the equations of motion with a 2-fs time step, each system was initially equilibrated by the Langevin thermostat in NVT-ensemble (50 ps) and then in NpT-ensemble (500 ps). The first 5 ns of the actual simulations were run in NpT-ensemble ($T = 310$ K, $p = 1$ atm) using the Berendsen thermostat and barostat [83], after which we switched to the Nosé-Hoover thermostat and the Parrinello–Rahman barostat to produce the correct ensemble. The pressure coupling was applied in a semi-isotropic way to result in zero surface tension. The long-range electrostatic interactions were accounted for by the reaction-field method (with $r_c = 2.0$ nm) and a 1.0-nm cutoff was used for the Lennard–Jones interactions. Reaction-field has been shown to be a reliable and well-scalable method for simulating noncharged lipid bilayers [84]. The simulation time was 100 ns for S_A and S_B, but 50 ns for system S_C, which together took about ten cpu-years on a parallel machine. For the analysis, we have included the last 40 ns of each simulation trajectory whenever not indicated otherwise.

The equilibration of the bilayer structure was monitored by the area per lipid (see Figure S1). The magnitude of area fluctuations were used to estimate the area compressibility of each bilayer [85]. The average bilayer thickness was estimated from the peak-to-peak distance of the electron density plot of all atoms across the simulation box. To characterize undulatory and peristaltic motions, we followed the procedure by Lindahl and Edholm [30], in which a grid was fitted to selected atoms in the POPC and PSM backbone (glycerol C2 in POPC and the corresponding carbon in PSM). The grids for the two monolayers were then averaged for undulatory analysis whereas their difference was used for describing the peristaltic motions, and in both cases 2-D FFT was applied to the grid points. k_c was estimated by summing over the undulatory spectral modes and utilizing the formula $<u^2_{und}> \approx k_B TA/(8.3\pi^3 k_c)$. Consistent results for k_c were found through a fit to the function $u^2_{und}(k) \sim k^{-4}$.

The deuterium (NMR)–order parameter S_{CD} values were calculated from the diagonal elements of the molecular order tensor (see [84]) at selected carbon locations of the PSM and POPC chains. To characterize the lateral heterogeneity in the system, carbons 5–7 were chosen from each acyl chain (together with the structurally correspondent carbons from the sphingosine chain), and the instantaneous S_{CD} values were binned on a grid on the bilayer plane. Similarly, the average in-plane electron densities were calculated by binning the number of electrons in the selected molecules or atoms. For the 2-D radial distribution functions, $g_{2D}(r)$, we used the projected center of mass positions of the lipid molecules. The centers of mass were also used to obtain the lateral diffusion coefficients (for details see [15]).

Finally, lateral pressure profiles were determined using an approach similar to the ones presented and validated by several authors [19,60–62], more details of our method in [86]. The lateral pressure was calculated using the Irving–Kirkwood contour and dividing the systems in ~0.1 nm thick slabs (100 slabs). Pairwise forces were calculated from the force field description and MD trajectory. A 2.0-nm truncation was used for electrostatic interactions. Constrained forces arising from SETTLE and LINCS were calculated from the general equation by Hess et al. [87]. As undulations in system S_C render the lateral pressure calculation more difficult, we chose three previous simulations on single-component lipid systems,

POPC [86], PSM [34], and a binary 1:4 DPPC–CHOL [17] for reference. For each system, the pressure profile was calculated the same way. To estimate the effect of pressure profile on membrane proteins, we followed the approach introduced by Cantor [88] and later applied to molecular simulation data of single-component bilayers by Gullingsrud et al. [62]. As a model we use the mechanosensitive ion channel MscL, whose conformation has been found to change anisotropically between cylindrical (open) and cone (closed) shapes [89]. Here we calculate the work, ΔW, done against the lateral pressure profile to alter the shape of the membrane cavity occupied by the protein as it changes conformation from the closed to an open state. Then ΔW can be written as:

$$\Delta W = \int p(z)\,\Delta A(z)\,dz, \qquad (1)$$

where $\Delta A(z)$ is the change in the cross-sectional area of the protein and $p(z)$ is the pressure profile. Here, we use an approach identical to that used in [62], and identical values for $\Delta A(z)$ for MscL as used in [62], in which the area is kept unchanged in the middle of the membrane between the two states. Error bars for ΔW have been calculated using results for different monolayers. It is, however, important to realize that ΔW depends on the second moment of the lateral pressure profile [62] and thus is susceptible to small changes of lateral pressure far from the bilayer center. Therefore, extra caution must be followed when interpreting these results. Also, in this approach the influence of inserting a protein into the membrane on the lateral pressure profile is not taken into account.

Supporting Information

Figure S1. The Area per Lipid versus Simulation Time

Found at doi:10.1371/journal.pcbi.0030034.sg001 (509 KB EPS).

Figure S2. Averaged Snapshots from the Last 10 ns of Each Simulation

The data is represented as in Figure 2 of the main article, but plotted for the top monolayer (columns 1–3) instead of the bottom monolayer.

Found at doi:10.1371/journal.pcbi.0030034.sg002 (212 KB EPS).

Figure S3. Snapshots (1-ns Averages) Revealing the In-Plane Electron Density of CHOL at 10-ns Time Intervals

Columns A1–C1 are the bottom monolayer and columns A2–C2 the top monolayer in systems S_A to S_C, respectively.

Found at doi:10.1371/journal.pcbi.0030034.sg003 (1.2 MB EPS).

Figure S4. Snapshots (1-ns Averages) Revealing the Undulation and Peristaltic Motions at 10-ns Time Intervals

Columns A1–C1 are the average bilayer height ($z(x,y)$, the mean height of the two monolayers), whereas columns A2–C2 are the bilayer thickness ($d(x,y)$, the difference in height of the two monolayers) in systems S_A to S_C, respectively. For calculating $z(x,y)$ and $d(x,y)$, we used the grid method discussed in the Methods section.

Found at doi:10.1371/journal.pcbi.0030034.sg004 (725 KB EPS).

Figure S5. Undulatory Spectral Intensity per Wave Mode versus Wave Vector Magnitude for Systems S_A to S_C

The legend shows k_c values calculated by two different methods, the summing method utilizing Equation 4 and fitting Equation 3 in [30].

Found at doi:10.1371/journal.pcbi.0030034.sg005 (183 KB EPS).

Figure S6. Peristaltic Spectral Intensity per Wave Mode versus Wave Vector Magnitude for Systems S_A to S_C

Found at doi:10.1371/journal.pcbi.0030034.sg006 (97 KB EPS).

References

1. Singer SJ, Nicolson GL (1972) The fluid mosaic model of the structure of cell membranes. Science 175: 720–731.
2. Simons K, Ikonen E (1997) Functional rafts in cell membranes. Nature 387: 569–572.
3. Edidin M (2003) The state of lipid rafts: From model membranes to cells. Annu Rev Biophys Biomol Struct 32: 257–283.
4. Pike LJ (2004) Lipid rafts: Heterogeneity on the high seas. Biochem J 378: 281–292.
5. Hancock JF (2006) Lipid rafts: Continuous only from simplistic standpoints. Nat Rev Mol Cell Biol 7: 456–462.
6. Simons K, Vaz WLC (2004) Model system, lipid rafts, and cell membranes. Annu Rev Biophys Biomol Struct 33: 269–295.
7. Gaus K, Gratton E, Kable EPW, Jones AS, Gelissen I, et al. (2003) Visualizing lipid structure and raft domains in living cells with two-photon microscopy. Proc Natl Acad Sci U S A 100: 15554–15559.
8. Brown RE (1998) Sphingolipid organization in biomembranes: What physical studies of model membranes reveal. J Cell Sci 111: 1–9.
9. London E (2005) How principles of domain formation in model membranes may explain ambiguities concerning lipid raft formation in cells. Biochim Biophys Acta 1746: 203–220.
10. Almeida PFF, Pokorny A, Hinderliter A (2005) Thermodynamics of membrane domains. Biochim Biophys Acta 1720: 1–13.
11. Shaikh SR, Edidin MA (2006) Membranes are not just rafts. Chem Phys Lipids 144: 1–3.
12. Hevonoja T, Pentikäinen MO, Hyvönen MT, Kovanen PT, Ala-Korpela M (2000) Structure of low density lipoprotein (LDL) particles: Basis for understanding molecular changes in modified LDL. Biochim Biophys Acta 1488: 189–210.
13. Ramstedt B, Slotte JP (2002) Membrane properties of sphingomyelins. FEBS Lett 531: 33–37.
14. Holopainen JM, Metso AJ, Mattila JP, Jutila A, Kinnunen PKJ (2004) Evidence for the lack of a specific interaction between cholesterol and sphingomyelin. Biophys J 86: 1510–1520.
15. Falck E, Patra M, Karttunen M, Hyvönen MT, Vattulainen I (2004) Lessons of slicing membranes: Interplay of packing, free area, and lateral diffusion in phospholipid/cholesterol bilayers. Biophys J 87: 1076–1091.
16. Hofsäss C, Lindahl E, Edholm O (2003) Molecular dynamics simulations of phospholipid bilayers with cholesterol. Biophys J 84: 2192–2206.
17. Vainio S, Jansen M, Koivusalo M, Róg T, Karttunen M, et al. (2006) Significance of sterol structural specificity. Desmosterol cannot replace cholesterol in lipid rafts. J Biol Chem 281: 348–355.
18. Kupiainen M, Falck E, Ollila S, Niemelä P, Gurtovenko AA, et al. (2005) Free volume properties of sphingomyelin, DMPC, DPPC, and PLPC bilayers. J Comput Theor Nanosci 2: 401–413.
19. Patra M (2005) Lateral pressure profiles in cholesterol–dppc bilayers. Eur Biophys J 35: 79–88.
20. Cantor RS (1997) The lateral pressure profile in membranes: A physical mechanism of general anesthesia. Biochemistry 36: 2339–2344.
21. Varma R, Mayor S (1998) GPI-anchored proteins are organized in submicron domains at the surface. Nature 394: 798–801.
22. Plowman SJ, Muncke C, Parton RG, Hancock JF (2005) H-ras, K-ras, and inner plasma membrane raft proteins operate in nanoclusters with differential dependence on the actin cytoskeleton. Proc Natl Acad Sci U S A 102: 15500–15505.
23. Pandit SA, Jakobsson E, Scott HL (2004) Simulation of the early stages of nano-domain formation in mixed bilayers of sphingomyelin, cholesterol, and dioleylphosphatidylcholine. Biophys J 87: 3312–3322.
24. Pandit SA, Vasudevan S, Chiu SW, Mashl RJ, Jakobsson E, et al. (2004) Sphingomyelin–cholesterol domains in phospholipid membranes: Atomistic simulation. Biophys J 87: 1092–1100.
25. Cantor RS (1997) Lateral pressures in cell membranes: A mechanism for modulation of protein function. J Phys Chem B 101: 1723–1725.
26. Templer RH, Castle SJ, Curran AR, Rumbles G, Klug DR (1998) Sensing isothermal changes in the lateral pressure in model membranes using dipyrenyl phosphatidylcholine. Faraday Discuss 111: 41–53.
27. de Almeida RFM, Fedorov A, Prieto M (2003) Sphingomyelin/phosphatidylcholine/cholesterol phase diagram: Boundaries and composition of lipid rafts. Biophys J 85: 2406–2416.
28. Patra M, Salonen E, Terama E, Vattulainen I, Faller R, et al. (2006) Under

the influence of alcohol: The effect of ethanol and methanol on lipid bilayers. Biophys J 90: 1121–1135.

29. Kucerka N, Tristram-Nagle S, Nagle JF (2005) Structure of fully hydrated fluid phase lipid bilayers with monounsaturated chains. J Membrane Biol 208: 193–202.

30. Lindahl E, Edholm O (2000) Mesoscopic undulations and thickness fluctuations in lipid bilayers from molecular dynamics simulations. Biophys J 79: 426–433.

31. Evans E, Rawicz W (1990) Entropy driven tension and bending elasticity in condensed-fluid membranes. Phys Rev Lett 64: 2094–2097.

32. Rawicz W, Olbrich KC, McIntosh T, Needham D, Evans E (2000) Effect of chain length and unsaturation on elasticity of lipid bilayers. Biophys J 79: 328–339.

33. Filippov A, Orädd G, Lindblom G (2003) The effect of cholesterol on the lateral diffusion of phospholipids in oriented bilayers. Biophys J 84: 3079–3086.

34. Niemelä P, Hyvönen MT, Vattulainen I (2004) Structure and dynamics of sphingomyelin bilayer: Insight gained through systematic comparison to phosphatidylcholine. Biophys J 87: 2976–2989.

35. Filippov A, Orädd G, Lindblom G (2004) Lipid lateral diffusion in ordered and disordered phases in raft mixtures. Biophys J 86: 891–896.

36. McIntosh TJ (1978) The effect of cholesterol on the structure of phosphatidylcholine bilayers. Biochim Biophys Acta 513: 43–58.

37. Sankaram MB, Thompson TE (1990) Modulation of phospholipid acyl chain order by cholesterol. A solid-state 2H nuclear magnetic resonance study. Biochemistry 29: 10676–10684.

38. Smaby JM, Momsen M, Kulkarni VS, Brown RE (1996) Cholesterol-induced interfacial area condensations of galactosylceramides sphingomyelins with identical acyl chains. Biochemistry 35: 5696–5704.

39. Needham D, McIntosh TJ, Evans E (1988) Thermomechanical and transition properties of dimyristoylphosphatidylcholine/cholesterol bilayers. Biochemistry 27: 4668–4673.

40. Niemelä P, Hyvönen MT, Vattulainen I (2006) Influence of chain length and unsaturation on sphingomyelin bilayers. Biophys J 90: 851–863.

41. Needham D, Nunn RS (1990) Elastic deformation and failure of lipid bilayer membranes containing cholesterol. Biophys J 58: 997–1009.

42. Henriksen J, Rowat AC, Ipsen JH (2004) Vesicle fluctuation analysis of the effect of sterols on membrane bending rigidity. Eur Biophys J 33: 732–741.

43. Rinia HA, Snel MME, van der Eerden JPJM, de Kruijff B (2001) Visualizing detergent resistant domains in model membranes with atomic force microscopy. FEBS Lett 501: 92–96.

44. Filippov A, Orädd G, Lindblom G (2006) Sphingomyelin structure influences the lateral diffusion and raft formation in lipid bilayers. Biophys J 90: 2086–2092.

45. Clarke JA, Heron AJ, Seddon JM, Law RW (2006) The diversity of the liquid ordered (l_o) phase of phosphatidylcholine/cholesterol membranes: A variable temperature multinuclear solid-state nmr and X-ray diffraction study. Biophys J 90: 2383–2393.

46. Jensen MO, Mouritsen OG (2004) Lipids do influence protein function—The hydrophobic matching hypothesis revisited. Biochim Biophys Acta 1666: 205–226.

47. McIntosh TJ, Simon SA (2006) Roles of bilayer material properties in function and distribution of membrane properties. Annu Rev Biophys Biomol Struct 35: 177–198.

48. Perozo E, Kloda A, Cortes DM, Martinac B (2002) Physical principles underlying the transduction of bilayer deformation forces during mechanosensitive channel gating. Nature Struct Biol 9: 696–703.

49. Hong H, Tamm LK (2004) Elastic coupling of integral membrane protein stability to lipid bilayer forces. Proc Natl Acad Sci U S A 101: 4065–4070.

50. Kuzmin PI, Akimov SA, Chizmadzhev YA, Zimmerberg J, Cohen FS (2005) Line tension and interaction energies of membrane rafts calculated from lipid splay and tilt. Biophys J 88: 1120–1133.

51. Zhelev DV (1998) Material property characteristics for lipid bilayers containing lysolipid. Biophys J 75: 321–330.

52. Allende D, McIntosh TJ (2003) Mellitin-induced bilayer leakage depends on lipid material properties: Evidence for toroidal pores. Biophys J 88: 1828–1837.

53. Seelig J, Waespe-Sarcevic N (1978) Molecular order in cis and trans unsaturated phospholipid bilayers. Biochemistry 17: 3310–3315.

54. Mehnert T, Jacob K, Bittman R, Beyer K (2006) Structure and lipid interaction of N-palmitoylsphingomyelin in bilayer membranes as revealed by 2H-NMR spectroscopy. Biophys J 90: 939–946.

55. Guo W, Kurze V, Huber T, Afdhal NH, Beyer K, et al. (2002) A solid-state NMR study of phospholipid–cholesterol interactions: Sphingomyelin–cholesterol binary systems. Biophys J 83: 1465–1478.

56. Pitman MC, Suits F, MacKerell AD Jr, Feller SE (2004) Molecular-level organization of saturated and polyunsaturated fatty acids in a phosphatidylcholine bilayer containing cholesterol. Biochemistry 43: 15318–15328.

57. Róg T, Pasenkiewicz-Gierula M (2006) Cholesterol–sphingomyelin interactions: A molecular dynamics simulation study. Biophys J 91: 3756–3767.

58. Aittoniemi J, Niemelä PS, Hyvonen MT, Karttunen M, Vattulainen I (2007) Insight into the putative specific interactions between cholesterol, sphingomyelin and palmitoyl–oleoyl phosphatidylcholine. Biophys J 92: 1125–1127.

59. Eckenhoff RG (2001) Promiscuous ligands and attractive cavities. How do the inhaled anesthetics work? Mol Interv 1: 258–268.

60. Lindahl E, Edholm O (2000) Spatial and energetic–entropic decomposition of surface tension in lipid bilayers from molecular dynamics simulations. J Chem Phys 113: 3882–3893.

61. Sonne J, Hansen FY, Peters GH (2005) Methodological problems in pressure profile calculations for lipid bilayers. J Chem Phys 122: 124903.

62. Gullingsrud J, Schulten K (2004) Lipid bilayer pressure profiles and mechanosensitive channel gating. Biophys J 86: 3496–3509.

63. Carrillo-Tripp M, Feller SE (2005) Evidence for a mechanism by which ω-3 polyunsaturated lipids may affect membrane protein function. Biochemistry 44: 10164–10169.

64. Cantor RS (1998) The lateral pressure profile in membranes: A physical mechanism of general anesthesia. Toxicol Lett 100–101: 451–458.

65. Sukharev SI, Sigurdson WJ, Kung C, Sachs F (1999) Energetic and spatial parameters for gating of the bacterial large conductance mechanosensitive channel, MscL. J Gen Physiol 113: 525–593.

66. Doyle DA (2004) Structural changes during ion channel gating. Trends Neurosci 27: 298–302.

67. van den Brink–van der Laan E, Killian JA, de Kruijff B (2004) Nonbilayer lipids affect peripheral and integral membrane proteins via changes in the lateral pressure profile. Biochim Biophys Acta 1666: 275–288.

68. Bezrukov SM (2000) Functional consequences of lipid packing stress. Curr Opin Coll Int Sci 5: 237–243.

69. Lewis JR, Cafiso DS (1999) Correlation of the free energy of a channel-forming voltage-gated peptide and the spontaneous curvature of bilayer lipids. Biochemistry 38: 5932–5938.

70. Meyer GR, Gullingsrud J, Schulten K, Martinac B (2006) Molecular dynamics study of MscL interactions with a curved lipid bilayer. Biophys J 91: 1630–1637.

71. Botelho AV, Gibson NJ, Thurmond RL, Wang Y, Brown MF (2002) Conformational energetics of rhodopsin modulated by nonlamellar-forming lipids. Biochemistry 41: 6354–6368.

72. Troost J, Lindenmaier H, Haefeli WE, Weiss J (2004) Modulation of cellular cholesterol alters p-glycoprotein activity in multidrug-resistant cells. Mol Pharmacol 66: 1332–1339.

73. Kamau SW, Krämer SD, Günthert M, Wunderli-Allenspach H (2005) Effect of the modulation of the membrane lipid composition on the localization and function of p-glycoprotein in MDR1-MDCK cells. In Vitro Cell Dev Biol Anim 41: 207–216.

74. Powl AM, Carney J, Maurius P, East JM, Lee AG (2005) Lipid interactions with bacterial channels: Fluorescence studies. Biochem Soc Trans 33: 905–909.

75. Palsdottir H, Hunte C (2004) Lipids in membrane protein structures. Biochim Biophys Acta 1666: 2–18.

76. Henriksen J, Rowat AC, Brief E, Hsueh YW, Thewalt JL, et al. (2006) Universal behavior of membranes with sterols. Biophys J 90: 1639–1649.

77. van den Brink–van der Laan E, Chupin V, Killian JA, de Kruijff B (2004) Small alcohols destabilize the KcsA tetramer via their effect on the membrane lateral pressure. Biochemistry 43: 5937–5942.

78. Safran S (1994) Frontiers in physics. Volume 90. Statistical thermodynamics of surfaces, interfaces, and membranes. New York: Addison-Wesley. 498 p.

79. Tieleman DP, Berendsen HJC (1998) A molecular dynamics study of the pores formed by Escherichia coli OmpF porin in a fully hydrated palmitoyloleoylphosphatidylcholine bilayer. Biophys J 74: 2786–2801.

80. Höltje M, Förster T, Brandt B, Engels T, von Rybinski W, et al. (2001) Molecular dynamics simulations of stratum corneum lipid models: Fatty acids and cholesterol. Biochim Biophys Acta 1511: 156–167.

81. Berendsen HJC, Postma JPM, van Gunsteren WF, Hermans J (1981) Interaction models for water in relation to protein hydration. In: Pullman B, editor. Intermolecular forces. Dordrecht: Reidel. pp. 331–342.

82. Lindahl E, Hess B, van der Spoel D (2001) Gromacs 3.0: A package for molecular simulation and trajectory analysis. J Mol Mod 7: 306–317.

83. Berendsen HJC, Postma JPM, van Gunsteren WF, DiNola A, Haak JR (1984) Molecular dynamics with coupling to an external bath. J Chem Phys 81: 3684–3690.

84. Patra M, Karttunen M, Hyvönen MT, Falck E, Vattulainen I (2004) Lipid bilayers driven to a wrong lane in molecular dynamics simulations by subtle changes in long-range electrostatic interactions. J Phys Chem B 108: 4485–4494.

85. Feller SE, Pastor RW (1999) Constant surface tension simulations of lipid bilayers: The sensitivity of surface areas and compressibilities. J Chem Phys 111: 1281–1287.

86. Ollila S (2006) Lateral pressure profile calculations of lipid membranes from atomic scale molecular dynamics simulations. [Master's thesis]. Helsinki: Helsinki University of Technology.

87. Hess B, Bekker H, Berendsen HJC, Fraaije JGEM (1997) LINCS: A linear constraint solver for molecular simulations. J Comput Chem 18: 1463–1472.

88. Cantor RS (1999) The influence of membrane lateral pressure on simple geometric models of protein conformational equilibra. Chem Phys Lipids 101: 45–56.

89. Sukharev S, Durell SR, Guy HR (2001) Structural models of the MscL gating mechanism. Biophys J 81: 917–936.

90. Thijsse BJ, Hollanders MA, Hendrikse J (1998) A practical algorithm for least-squares spline approximation of data containing noise. Comp Phys 12: 393–399.